Geometry and Structural Plasticity of Synaptic Connectivity

Armen Stepanyants,[1] Patrick R. Hof,[2]
and Dmitri B. Chklovskii[1,3]
[1]Cold Spring Harbor Laboratory
1 Bungtown Road
Cold Spring Harbor, New York 11724
[2]Kastor Neurobiology of Aging Laboratories
Fishberg Research Center for Neurobiology
Computational Neurobiology and Imaging Center
Advanced Imaging Program
and Departments of Geriatrics and Adult
Development, and Ophthalmology
Mount Sinai School of Medicine
New York, New York 10029

Summary

Changes in synaptic connectivity patterns through the formation and elimination of dendritic spines may contribute to structural plasticity in the brain. We characterize this contribution quantitatively by estimating the number of different synaptic connectivity patterns attainable without major arbor remodeling. This number depends on the ratio of the synapses on a dendrite to the axons that pass within a spine length of that dendrite. We call this ratio the filling fraction and calculate it from geometrical analysis and anatomical data. The filling fraction is 0.26 in mouse neocortex, 0.22–0.34 in rat hippocampus. In the macaque visual cortex, the filling fraction increases by a factor of 1.6–1.8 from area V1 to areas V2, V4, and 7a. Since the filling fraction is much smaller than 1, spine remodeling can make a large contribution to structural plasticity.

Introduction

Learning and memory rely on changes in neuronal circuits, or plasticity. An important contribution to neuronal plasticity comes from synapses. Traditionally, synaptic contributions to plasticity have been divided into the following categories (Bailey and Kandel, 1993; Greenough and Bailey, 1988): changes in pre-existing synapses without alterations of interneuronal connectivity (Tanzi, 1893) and changes in interneuronal connectivity due to formation and elimination of synapses (Ramón y Cajal, 1893). The latter category can be further subdivided into contributions associated with dendritic spines without major remodeling of dendritic or axonal arbors (Dailey and Smith, 1996; Engert and Bonhoeffer, 1999; Lendvai et al., 2000; Maletic-Savatic et al., 1999; Toni et al., 1999), and contributions associated with remodeling of dendritic and axonal branches (Baker and Van Pelt, 1997; Darian-Smith and Gilbert, 1994; Greenough et al., 1985; Harris and Woolsey, 1981; O'Rourke and Fraser, 1990; Petit et al., 1988; Purves and Hadley, 1985; Purves et al., 1986; Rajan and Cline, 1998; Rajan et al.,

1999; Stern and Armstrong, 1998; Witte et al., 1996; Wong et al., 2000; Woolley, 1999).

The three resulting categories of synaptic contributions to plasticity occur on distinct time scales. The fastest contribution is synaptic strength change, which can be realized within a minute (Bliss and Collingridge, 1993; Gustafsson and Wigstrom, 1990; Madison et al., 1991; Malinow et al., 2000). Formation of new spines takes longer, on the order of tens of minutes (Dailey and Smith, 1996; Engert and Bonhoeffer, 1999; Lendvai et al., 2000; Maletic-Savatic et al., 1999; Toni et al., 1999). Finally, major branch remodeling is the slowest process, usually occurring on the time scale of days (Baker and Van Pelt, 1997; Darian-Smith and Gilbert, 1994; Greenough et al., 1985; Harris and Woolsey, 1981; O'Rourke and Fraser, 1990; Petit et al., 1988; Purves and Hadley, 1985; Purves et al., 1986; Rajan and Cline, 1998; Rajan et al., 1999; Stern and Armstrong, 1998; Witte et al., 1996; Woolley, 1999), although some changes may happen faster (Wong et al., 2000).

Distinct time scales associated with these three categories of synaptic plasticity justify analyzing them separately. Such analysis should help in understanding these categories' respective roles in learning and memory. Here, we attempt to make a step in this direction by analyzing one of the categories: dendritic spine remodeling.

The goal of this study is to characterize quantitatively the potential for plasticity associated with formation and elimination of dendritic spines only. To do this, we estimate the number of different interneuronal connectivity patterns that can be implemented without major remodeling of axonal and dendritic arbors. This number places an upper bound on the plasticity associated with spine remodeling. In other words, the number of different synaptic connectivity patterns gives the maximum capacity of memory associated with formation and elimination of dendritic spines.

The number of different synaptic patterns does not just depend on the number of existing synapses but also on the number of potential synaptic locations. We refer to these locations as potential synapses (Figure 1). Knowing the number of the potential synapses is crucial in estimating the number of different synaptic patterns. We illustrate this point in Figure 1 and Table 1 with a simple example with three actual synapses, $N = 3$. If the number of potential synapses is close to the number of actual synapses, then there is almost no room for changes in connectivity and the number of different synaptic patterns is small (Figure 1B). If the number of potential synapses is much greater than the number of actual synapses (Figure 1C), then there are plenty of different connectivity patterns that can be implemented by spine rearrangement (Figure 1D).

We estimate the number of potential synapses by calculating the number of axons that pass within the spine length from a dendrite. We show through a geometrical analysis that this number can be expressed in terms of experimentally measurable anatomical parameters, independent of the details of arbor geometry. This

[3] Correspondence: mitya@cshl.org

filling fraction, $f = ?$ filling fraction, $f = 1$
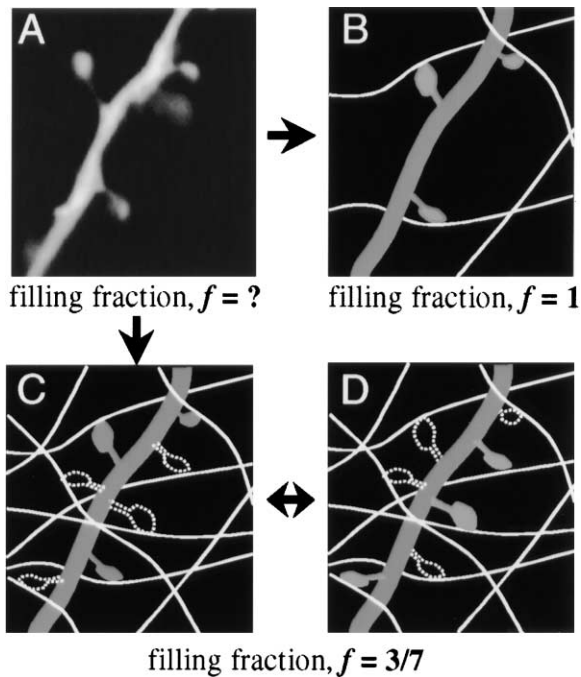
filling fraction, $f = 3/7$

Figure 1. Structural Plasticity of Synaptic Connectivity Patterns

(A) Light microscopy image of a typical spiny dendrite.

(B) Schematic drawing showing the dendrite in (A) together with nearby axons in one possible scenario. In this scenario, spine remodeling cannot contribute to circuit reorganization because all axons within the spine length of a dendrite are taken.

(C) The same dendrite in another scenario, where spine remodeling can contribute to circuit reorganization. Actual dendritic spines (solid gray) form actual synapses. Potential synapses include both actual synapses and possible spine locations (dashed contours).

(D) Another possible synaptic connectivity pattern attainable from (C) by spine remodeling. Our calculations show that the real brain is more like scenario (C) rather than scenario (B). The total number of different available synaptic connectivity patterns characterizes the plasticity potential and gives the upper bound for the memory capacity associated with spine remodeling.

allows us to estimate the number of potential synapses from the values of dendritic length per neuron, spine length, interbouton interval, and of synaptic density. Using this estimate, we calculate the number of different patterns of connectivity and the memory capacity associated with them.

Our results can be concisely expressed in terms of a single parameter: the filling fraction, f, given by the ratio of actual to potential synapses. The filling fraction characterizes the potential for altering neuronal circuits through formation and elimination of dendritic spines. High filling fraction implies little plasticity potential
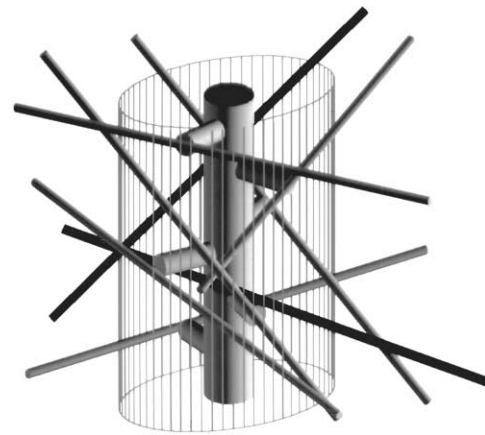

Figure 2. Geometry of Synaptic Connectivity for Random Orientation of Axons

The cylinder around the dendrite indicates the space within spines' reach. Its radius is defined by spine length, as measured from the dendritic axis. Intrinsic and extrinsic projections are shown in gray and black, respectively.

whereas low filling fraction implies a high plasticity potential.

Results

Expression for the Number of Potential Synapses

To estimate the number of potential synapses on a dendrite, we calculate the number of axons that course within a spine's length of the dendrite. We follow the suggestion of Swindale (1981), and imagine a cylinder centered on the dendritic axis, with its radius equal to the spine length (as measured from the dendritic axis to the tip of the spine, Figure 2). Then, all of those axons (and only those) that intersect the cylinder may form a synapse with the dendrite. Therefore, we need to calculate the number of axons intersecting this cylinder. Below we present our calculations for three situations of sequentially increasing realism and complexity.

First, consider a simplified situation where all axons course in the same direction, which is perpendicular to the axis of the cylinder (Figure 3). Then, imagine a rectangular box with dimensions of axonal length per neuron, L_a (parallel to the axons), dendritic length per neuron, L_d (parallel to the dendrite), and two spine lengths, $2s$. All of those neurons (and only those), whose somata centers are located within the box, have axons intersecting the cylinder. Therefore, the number of eligible axons, and, hence, the number of potential synapses per neuron, N_P, is given by the product of the box volume and the neuronal density, n:

$$N_P = 2sL_dL_an \qquad (1)$$

Second, consider a more realistic situation where local axons travel in different directions (Figure 2). Assuming that axonal directions are distributed isotropically relative to the dendrite, we can average over possible directions to find the total number of axons intersecting the cylinder and hence, the number of potential synapses (see Experimental Procedures):

Table 1. The Number of Different Synaptic Connectivity Patterns

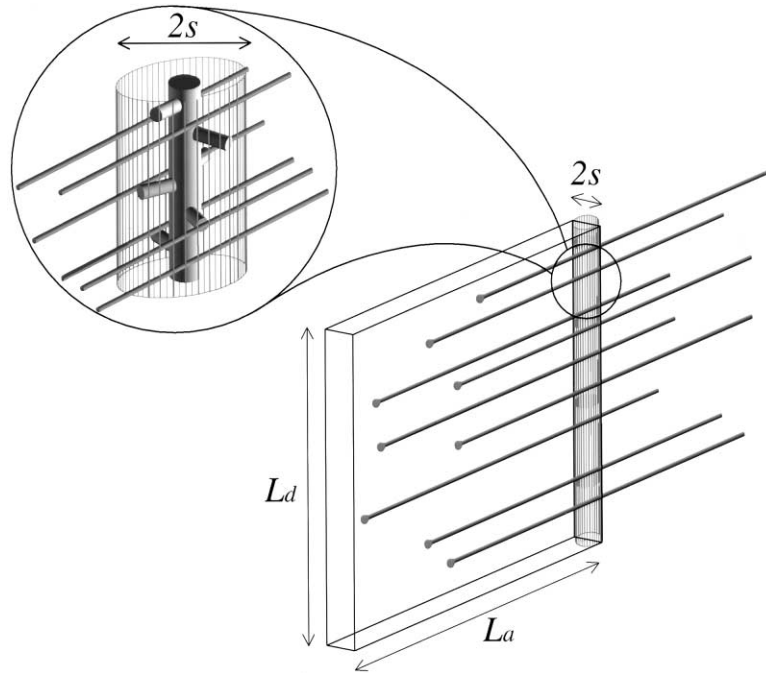| Number of Potential Synapses, N_P	Filling Fraction, $f = N/N_P$	Number of Patterns, $C_{N_P}^{N}$
3	1	1
4	0.75	4
5	0.6	10
7	0.43	35
10	0.3	120

Figure 3. Geometry of Synaptic Connectivity in a Simplified Case of Axons Running in the Same Direction, Perpendicular to Dendritic Axis

The blow up shows the relation between a spiny dendritic segment and axons. The main figure shows a box that contains the centers of cell bodies whose axons hit the cylinder around the dendrite. The number of these axons gives an estimate for the number of potential synapses.

$$N_P = \frac{\pi}{2} s L_d L_a n \qquad (2)$$

Notice that the only difference between Equations 1 and 2 is in the numerical factor ($2 \rightarrow \pi/2$). According to Equation 2, one can view the number of potential synapses, N_P, as the product of the dendritic cross-section (by the dendritic cross-section here we mean the dendritic arbor footprint area as seen by a passing axon), $\pi/2\, sL_d$, and axon density, $L_a n$. However, the utility of this expression is somewhat limited because it takes into account only local axonal inputs through the local axon density, $L_a n$.

Third, we generalize Equation 2 to include both local and nonlocal axons (i.e., axons belonging to remote cell bodies [Figure 2]). To do this, we replace the local axon density, $L_a n$, with the total axon density, which includes both local and nonlocal inputs. The total axon density can be written as the product of the average interbouton distance, b, and synapse density, n_s. This amounts to the substitution $L_a n \rightarrow bn_s$ in Equation 2 (for details, see Experimental Procedures):

$$N_P = \frac{\pi}{2} s L_d b n_s \qquad (3)$$

Next, we notice that the synapse density, n_s, can be expressed as the product of the neuron density, n, and the average number of synapses on a dendrite, N:

$$n_s = Nn \qquad (4)$$

Combining Equations 3 and 4, we arrive at the relation between the numbers of potential and actual synapses,

$$N_P = \frac{\pi}{2} s L_d b n N \qquad (5)$$

Because N_P is proportional to N, it is natural to introduce

a ratio of actual to potential synapses, f, which we call the filling fraction,

$$f = \frac{N}{N_P} = \frac{2}{\pi s L_d b n} \qquad (6)$$

Alternatively, f is a probability that two neurons form a synapse given that the presynaptic axon comes within the spine length of the postsynaptic dendrite. The filling fraction is by definition less than or equal to unity.

The derivation of Equation 6 is rather general. In particular, no assumptions are made about the shapes of dendritic and axonal arbors and the density of branches as a function of the distance to the cell body.

The derivation relies on the following realistic assumptions (see Experimental Procedures):

- We treat axons and dendrites as a collection of straight segments because the curvature radii of both axonal and dendritic branches are greater than spine length. This assumption holds for most neurons, including those in neocortex and hippocampus. This assumption is violated only in rare cases, such as, climbing fibers on Purkinje neurons in the cerebellum.
- Most axonal and dendritic branch segments are long compared to the spine length, thus justifying neglecting branch points in the geometry.
- We assume that the distribution of intersection angles between axons and dendrites is isotropic, which is already true for isotropic distribution of either axonal or dendritic branches. If the distribution of intersection angles were anisotropic, the numerical coefficient in the expression would be different. But as follows from comparing Equations 1 and 2, this coefficient does not vary much in realistic situations.
- Smallness of axonal diameter relative to the spine length justifies neglecting the volume exclusion effects between different axons.

- We assume that there is no correlation between axonal density and dendrite location, i.e., axons are not on average "attracted to" or "repelled from" dendrites. Although this may not seem obvious, this assumption can be justified in the case of pyramidal neurons, as discussed in the next section.
- We only consider synapses among one type of spiny neurons, pyramidal cells. This is by far the dominant cell type in neocortex and hippocampus. For example, in the mouse neocortex, pyramidal cells make up 85% of the neuronal population, and 75% of all synapses reside on spines (Braitenberg and Schüz, 1998). Equations 3, 5, and 6 can be modified for the case of many different inputs, such as inputs from different populations of neurons like excitatory and inhibitory neurons, or geometrically different inputs like inputs to segregated parts of dendritic tree. This is considered in the Experimental Procedures section.
- We assume that the fraction of multiple synaptic boutons is small. This assumption is supported by the study of Jones (1999), who reported that the fraction of multiple synaptic boutons is 0.16 in the rat motor cortex, and studies of Yankova et al. (2001) and Sorra and Harris (1993), who found that in the rat hippocampus, this fraction is 0.18 and 0.24, respectively. For large fractions of multiple synaptic boutons, a correction has to be made to Equations 3, 5, and 6 (see Experimental Procedures).

Anatomical Estimates of the Ratio of Actual to Potential Synapses

The utility of Equation 6 is in relating the filling fraction, f, which would normally require laborious serial section electron-microscopic reconstructions, to the anatomical parameters measurable mostly by optical microscopy. In this section, we calculate the filling fraction from previously published anatomical data and our own measurements. Anatomical parameters used for our estimates along with the values of f are shown in Table 2.

First, we estimate the average value of f for the mouse neocortex using the data from the work of Braitenberg and Schüz (1998), Schüz and Palm (1989), and Hellwig et al. (1994) (Table 2). These authors carefully corrected their data for tissue shrinkage. We find that the ratio of actual to potential synapses is 0.26.

Second, we estimate the value of f for the rat hippocampus stratum oriens and stratum radiatum of CA3 and CA1 fields using the data from the work of Amaral et al. (1990), Shepherd et al. (2002), Shepherd and Harris (1998), Trommald et al. (1995), and Harris and Stevens (1989). The caveat here is that the pyramidal cell bodies in hippocampus are confined to a relatively thin layer (stratum pyramidale) rather than being distributed more uniformly in the volume. Hence, for the neuronal density in Equation 6 (see Experimental Procedures), we use the ratio of the total number of neurons to the combined volume of neuropil in stratum oriens and stratum radiatum, as provided in Boss et al. (1987) and West et al. (1978). In the CA3 field, the majority of synapses are made among local neurons, and we find that the filling fraction $f = 0.34$. There is additional complication for the CA1 field. Neurons in CA1 receive synapses not only from local neurons, but also from commissural axons

and Schaffer collaterals of CA3 neurons (CA3→CA1 projections). We find that for CA3→CA1 projections, only the filling fraction $f = 0.22$.

Third, we estimate the value of f for pyramidal neurons in the macaque visual pathways, in layer III of areas V1, V2, V4, and 7a (Table 2). Not having sufficient data for total dendritic length per neuron in these particular areas, we base our estimate on measurements from Elston and Rosa (1997, 1998), which include only the basal domain of the dendritic tree. These data are sufficient to estimate the relative values of f if we assume that the average dendritic length per layer III pyramidal neuron scales with basal dendritic length. This assumption is consistent with the available data from different cortical areas (Elston and Rosa, 1997; Page et al., 2002; Valverde, 1978) and our own observations, albeit obtained by different techniques. Typical morphologies of basal dendritic spines of layer III neurons in considered areas are shown in Figure 4. There are large differences in cytoarchitecture among these areas. According to our data, the neuronal density between areas V1 and 7a changes by more than a factor of two (Table 2, Figure 5). The average length of basal dendrites per neuron in different areas can differ by a factor of three with the lowest value in area V1 (Elston and Rosa, 1997, 1998). The number of spines on basal dendrites is about ten times higher along the temporal visual pathway than in area V1 (Elston, 2000). In spite of these large variations in microarchitecture, the ratio of actual to potential synapses f undergoes a lesser change from 0.12 in area V1 to 0.20–0.23 in areas V2, V4, and 7a. Because the data for the macaque monkey visual areas from Table 2 are not corrected for shrinkage, and the estimates of filling fraction are based on basal dendritic length, only the relative values (fractions) of filling fraction f among areas are reliable (see subsection on the robustness of the results).

Our estimates of f are influenced by variability among different brains and, to a smaller extent, by uncertainty in the measurements. Based on our data from five macaque monkeys (Table 2), the variability in pyramidal neuron density among different brains is 10%. The variability in average spine length is 3.5%. Unfortunately, the authors of the remainder of the data shown in Table 2 did not provide uncertainties to the listed average values. For this reason, we cannot calculate rigorously the uncertainty in the filling fraction f. However, we expect the variability in the average dendritic length per neuron and the average interbouton interval not to be much different from 3.5%–10%, and as a result the uncertainty in f is less than 20%. If this assumption is correct, then there are two significant differences in filling fraction: one between the CA3 and CA1 (CA3→CA1 projections) fields of the rat hippocampus, and another between the macaque monkey area V1 and areas V2, V4, and 7a. A more precise estimate of the uncertainties, in order to find significant differences among different brain areas and different species, will require future experiments.

In brain areas where the majority of synaptic connections originate from local neurons (intrinsic projections), Equation 2 can be used instead of Equation 6 to calculate the number of potential synapses N_P and the filling fraction f. This can be done for stratum oriens and stra-

Table 2. Anatomical Parameters of Excitatory Neurons and Corresponding Filling Fractions, f, for Different Species and Brain Areas

	Pyramidal Neuron Density n [10^4 mm^{-3}]	Dendritic Length/ Neuron L_d [mm]	Interbouton Interval b [μm]	Average Spine Length s [μm]	Filling fraction f
Mouse Neocortical Areas: MOs, VISp	7.8 (Braitenberg and Schüz, 1998; Schüz and Palm, 1989)	3.5 (Braitenberg and Schüz, 1998)	4.5 (Braitenberg and Schüz, 1998; Hellwig et al., 1994; Schüz and Palm, 1989)	2.0 (Braitenberg and Schüz, 1998; Spacek and Hartmann, 1983)	0.26
Rat hippocampal Areas:					
CA3	2.0 (Boss et al., 1987; West et al., 1987)	12.3 (Amaral et al., 1990)	4.2 (Shepherd et al., 2002)	1.8 (Harris and Stevens, 1989; Trommald et al., 1995)	0.34
CA1 (CA3→CA1 projections)	4.1 (Boss et al., 1987; West et al., 1978)	10.8 (Amaral et al., 1990)	3.7 (Shepherd and Harris, 1998)	1.8 (Harris and Stevens, 1989; Trommald et al., 1995)	0.22
Layer III of the Macaque Monkey Neocortical Areas:					
V1	22*	1.4 (Elston and Rosa, 1997)	6.4 (Amir et al., 1993)	2.6*	0.12
V2	13*	1.6 (Elston and Rosa, 1998; Elston and Rosa, 1997)	6.4 (Amir et al., 1993)	2.1*	0.23
V4	11*	2.1 (Elston and Rosa, 1998)	6.4 (Amir et al., 1993)	2.2*	0.20
7a	8.0*	2.6 (Elston and Rosa, 1997)	6.4 (Amir et al., 1993)	2.1*	0.23

Asterisks denote original data. Macaque value of L_d is the total length of basal dendrities per layer III neuron. Only the relative values of filling fraction f for Macaque areas are reliable (see the text for details).

tum radiatum of CA3, where the majority of synapses are made among CA3 neurons (Amaral et al., 1990). The same can be done for the primary visual cortex in primates, where the extrastriate cortical input amounts to 11% of the total excitatory input (Budd, 1998). However, Equation 2 may fail if applied to prefrontal or other association cortices, where the extrinsic input is not necessarily small. In these areas, a more general expression, i.e., Equation 6, may be used instead.

Anatomical data allow us to verify an assumption made in the derivation of Equation 6 that the axonal density can be treated as uniform on the length scale of a few spine lengths. A possible objection is that axons are attracted to dendrites, and therefore the number of potential synapses is greater than estimated. For pyramidal neurons, this is not a concern, however, because the density of dendrites is rather high in the brain. We estimate that each point on the axon falls within 3 to 4 different dendritic cylinders (this number is obtained by substituting parameters for mouse neocortex from Table 2 into the expression $\pi s^2 L_d n$). This means that at any point an axon can make a synapse with any of the 3 to 4 different dendrites. Therefore, even if an axon is deflected *toward* one dendrite, it will be effectively deflected *away* from some others. Thus, the density of axons is effectively uniform and the derivation of Equation 6 remains valid. However, such reasoning may fail for neurons other than pyramidal (e.g., when several neuronal types are involved) because of the low density

of dendrites. In this case, a blind application of Equation 6 may lead to the filling fraction value greater than one.

Information Storage Capacity of Synaptic Patterns

Here we use the values of the filling fraction, f, obtained in the previous section, to estimate the number of different synaptic connectivity patterns. This number places an upper bound on the plasticity potential, or memory capacity, associated with the formation and elimination of dendritic spines. Thus, it is natural to express our results in terms of the information storage capacity associated with changes in synaptic patterns. In this case, we use the notion of Shannon information (see for example Shannon and Weaver [1949]).

To estimate the information storage capacity associated with the synaptic connections of a given neuron, we calculate the number of ways by which one can choose N actual synapses out of N_P potential synapses. This number is given by the binomial coefficient, which, in the limit of large N, has the following form:

$$C_{N_P}^N = [(1 - f)^{1-f} f^f]^{-N_P} \qquad (7)$$

The information storage capacity is defined as the base two logarithm of the total number of different synaptic patterns:

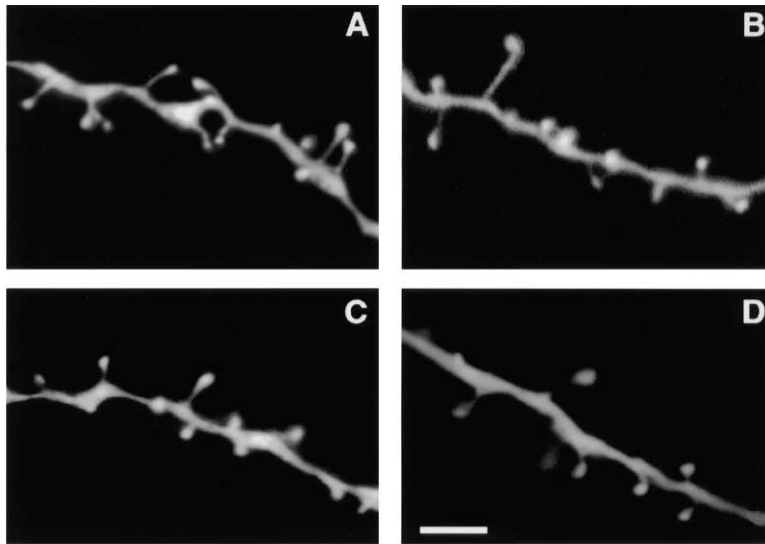$$I = -N_P[(1 - f) \log_2(1 - f) + f \log_2 f] \qquad (8)$$

Figure 4. Typical Morphology of Dendritic Spines on Lucifer Yellow-Loaded Corticocortically Projecting Layer III Neurons in the Macaque Monkey

Panel (A) shows a dendrite from a neuron located in area V1 projecting to area V2, panel (B) is from a neuron located in area V2 projecting to area V4, panel (C) is from a neuron located in area V4 projecting to the temporal cortex (area TEO), and panel (D) is from a neuron located in parietal area 7a projecting to prefrontal area 46. These pictures were obtained using a confocal microscope with a 100× objective and high zoom, and are single z planes. All dendritic segments shown in the figure are from basal dendrites. Similar materials were used to obtain the spine length distribution function (panel E), and to estimate the average spine length. Scale bar on (D) = 4 μm.
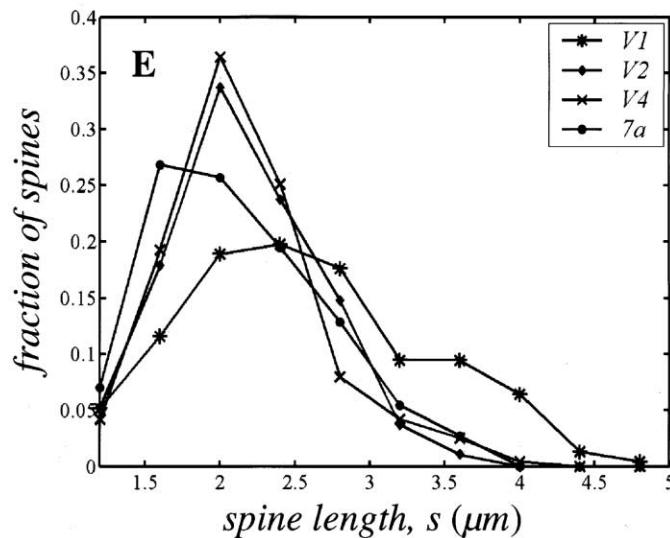
In the two limiting cases, when the filling fraction $f = 0$ or $f = 1$, the information storage capacity is zero because there is only one way to choose synaptic connections in these cases.

Because the information storage capacity scales with the number of synapses, it is useful to consider the information storage capacity per synapse I/N,

$$\frac{I}{N} = -\log_2 f - \frac{1-f}{f}\log_2(1-f) \qquad (9)$$

This expression is plotted in Figure 6. We note that this analysis is similar to the calculation of the information content of a spike train as discussed in Rieke et al. (1997), where an elegant and insightful explanation of information theoretical concepts in a neurobiological context can be found.

We estimate information storage capacity, due to spine remodeling only, Equation 9, by using the values for the filling fraction, f, from the previous section and find that each synapse may encode 3–4 bits of information (Table 2). This exceeds the naïve value of 1 bit per synapse because for each existing synapse, there are roughly four potential synapses that are not implemented. The calculated number of bits relates to the plasticity due to spine remodeling only, which, depending on the validity of several simplifying assumptions, could relate to the biologically meaningful memory capacity on corresponding time scale (see Discussion).

Robustness of the Results

It is important to validate our calculation of the filling fraction by comparison with direct electron microscopy measurements on serial sections. These measurements would yield local filling fraction values for particular dendrites rather than the mean value we calculate. Therefore, such comparison would require extensive sampling with electron microscopy, a rather laborious exercise. We would like to emphasize that the main value of the
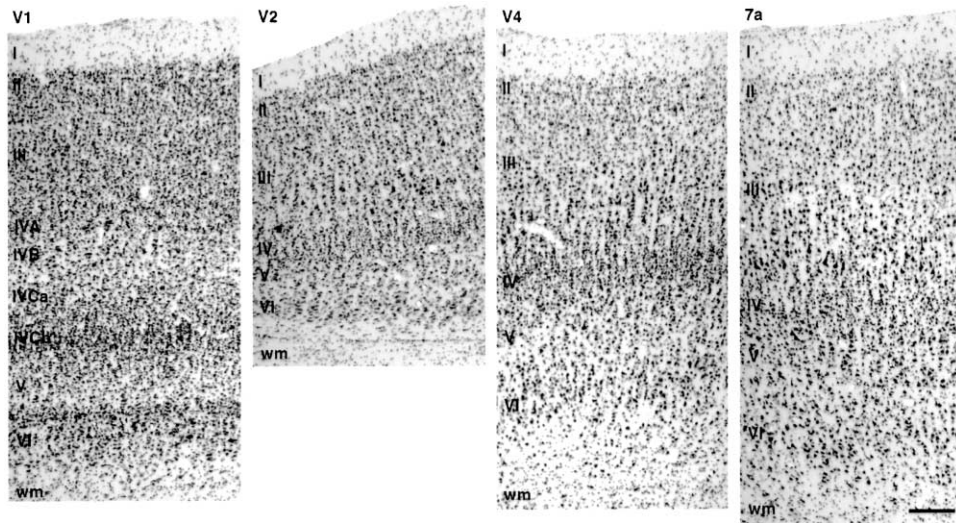
Figure 5. Cytoarchitecture of Cortical Areas V1, V2, V4, and 7a in the Macaque Monkey

Layer III neuron densities were obtained from similar preparations. Note the higher neuron density in area V1 compared to the three other regions. Although areas V2, V4, and 7a show differences in their cytoarchitecture, layer III neuronal densities are comparable among them. Materials were stained with cresyl violet and were photographed at the same magnification. Cortical layers are indicated by Roman numerals; wm, white matter. Scale bar on the right panel = 300 μm.

mathematical expression for the filling fraction is in determining the relative scaling of quantities involved rather than the exact numerical values.

When comparing different brain areas (e.g., 1 and 2) with each other, a relevant quantity is the relative filling fraction f_2/f_1. Therefore, in the measurements of neuronal density, interbouton interval, spine length, and dendritic length per neuron, it is not necessary to keep track of multiplicative corrections, as long as they are the same for the considered areas. This could include corrections for tissue shrinkage, multiple synaptic boutons, and correction of the geometrical factor $\overline{\sin(\theta_{ij})}$ for

non-isotropic distribution of angles among dendritic and axonal branches (see Experimental Procedures). This would also allow one to make estimates of the filling fraction based on a part of the dendritic tree (as it was done for the macaque visual cortex) provided the length of this part scales with the total dendritic length per neuron.

Because information capacity is usually defined up to an additive constant, a relevant quantity is the difference between information capacity of the two areas, or, more specifically, the relative information storage capacity per synapse, defined as $I_1/N_1 - I_2/N_2$. For small filling
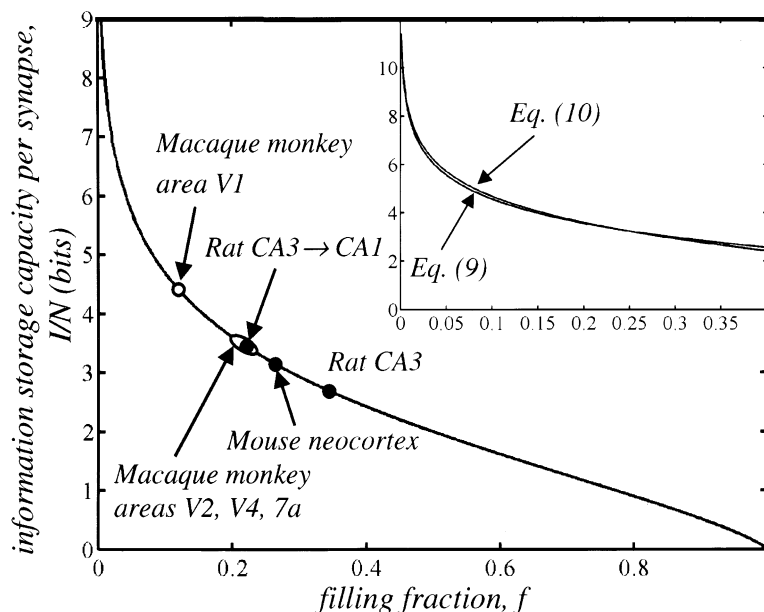

Figure 6. Information Storage Capacity per Synapse, Equation 9, versus the Filling Fraction, f

The values of f for layer III of the macaque monkey neocortical areas (transparent symbols) are not corrected for shrinkage and are based on basal dendritic length per neuron only. As a result, only the relative information storage capacity per synapse (as defined by Eq. [11]) between area V1 and areas V2, V4, and 7a in the figure is reliable. The absolute values of information storage capacity per synapse for the macaque monkey should not be compared to rat hippocampus and mouse neocortex. The inset in the figure shows the comparison between Equation 9 and its approximation by Equation 10 for values of the filling fraction $f \leq 0.4$.

fraction, $f \leq 0.4$, the second term on the right side of Equation 9 varies between 1.44 and 1.11. This variation is small relative to the size of the first term and Equation 9 can be approximated by:

$$\frac{I}{N} \approx 1.25 - \log_2 f \qquad (10)$$

(for quality of this approximation see the inset in Figure 6). This implies the following relation between the relative information storage capacity and the relative filling fraction in the small filling fraction regime:

$$\frac{I_1}{N_1} - \frac{I_2}{N_2} \approx \log_2 \frac{f_2}{f_1} \qquad (11)$$

Because the data in Table 2 for the macaque monkey is not corrected for shrinkage, and L_d includes basal dendritic length only, we can only make two significant comparisons based on Equation 11: layer III of the macaque monkey area V1 encodes 0.7–0.9 bits more information per synapse than areas V2, V4, and 7a, and the stratum oriens and stratum radiatum in the CA1 (CA3→CA1 projections) field in rat hippocampus encode 0.7 bits more than in CA3.

Two comments are in order about the calculation of information storage capacity per synapse with Equations 9 and (10). First, the derivation of Equation 9 assumes the existence of a maximum spine length below which all connections are equally probable and above which they are impossible. However, our empirical assessment of the distribution of spine lengths revealed that it has a tail (Figure 4E). This means that in different samplings of spine lengths, the maximum spine length could be determined by outliers and is highly variable. To avoid this problem and obtain a meaningful definition of f and information capacity, we use the average spine length in our calculations. In fact, this choice is supported by the following analysis that takes into account the distribution of spine lengths. We calculated the information storage capacity per synapse based on the measured spine length distribution functions (Figure 4E) in layer III of the macaque monkey areas V1, V2, V4, and 7a. The results calculated in this way do not differ by more than 5% from those computed using Equations 9 or 10, where average spine lengths were used for calculation of filling fractions (results not shown).

Second, in estimating the information storage capacity associated with synaptic patterns, we assumed that a neuron forms a fixed number of actual synapses. In reality, the number of synapses per neuron is not strictly constant and can vary somewhat. Therefore, we estimate the increase in information capacity per synapse due to variability in the number of actual synapses. If a given neuron can make any number of synapses in the range from N to $N + \Delta N$ (we assume that $\Delta N \ll N$), then for realistic values of the filling fraction $f \leq 0.4$ the number of different synaptic patterns is limited from above:

$$\sum_{i=N}^{i=N+\Delta N} C_{N_p}^{i} < C_{N_p}^{N+\Delta N} \Delta N \qquad (12)$$

Taking the base two logarithm of this expression, and expanding the right-hand side of the inequality with respect to small $\Delta N/N$, we estimate that the increase in information capacity per synapse due to variability in N is small,

$$\Delta I < \log_2 \Delta N + \frac{\Delta N}{N} f \frac{\partial I}{\partial f} \ll I \qquad (13)$$

Discussion

Redundancies in the Circuitry

In the previous section, we calculated the number of geometrically different synaptic connectivity patterns. However, some geometrically different patterns of synaptic connectivity may result in topologically identical neuronal circuits. For example, in rat barrel cortex, connected neuronal pairs have an average of 3.4 synapses in layer IV and 5.5 synapses in layer V (Feldmeyer et al., 1999; Markram et al., 1997). The average number of potential synapses between two neurons can be even higher. Different ways of choosing actual synaptic connections out of potential ones could lead to identical circuits. Should these circuits be counted separately in the estimate of the information storage capacity?

The answer to this question depends on the model assumed for the propagation of the signal from the presynaptic to the postsynaptic neuron and integration of synaptic inputs in a dendrite. Here we discuss three popular hypotheses:

(1) No two different connectivity patterns between two neurons could lead to identical circuits. This could be due to the fact that difference in the location of a synapse on dendrite and axon could lead to the difference in delays in presynaptic axons, difference in attenuation in postsynaptic dendrite, etc. In this case, there is no degeneracy associated with different patterns of synaptic connectivity, and Equation 9 is valid.

(2) Synaptic inputs are summed linearly within dendritic compartments, which act as separate threshold units (Poirazi and Mel, 2001). Although in this case spine rearrangement within dendritic compartments could lead to degenerate connectivity patterns, it is unlikely for statistical reasons. Considering that on average there are only 3.4–5.5 synapses between a pair of neighboring connected neurons in the rat barrel cortex (Feldmeyer et al., 1999; Markram et al., 1997), the number of potential synapses between two neurons can be estimated as $N_p = N/f \approx 13 - 21$, using the filling fraction for mouse neocortex, $f = 0.26$. The number of dendritic compartments in these neurons is of the order of 100–150 (Feldmeyer et al., 1999; Markram et al., 1997). Hence, the average number of potential synapses between two neurons on a single dendritic compartment is of the order of 0.1 and is much smaller than 1. For this reason, it is unlikely that a single compartment has more than one potential synapse with any axon (unless there is a special mechanism that would allow presynaptic axons to target specific compartments), and the geometrically different circuits should be counted separately, as it is done in Equation 9.

(3) Postsynaptic current in the soma is independent of the position of the synaptic input on the dendritic arbor (Magee and Cook, 2000) and the summation of

inputs is linear (Cash and Yuste, 1999). In this case, different connectivity patterns between neurons would lead to identical circuitry, and Equation 9 is only an approximation. However, since the degenerate circuits should be counted only once in this case, the total number of different circuits will be smaller, and Equation 9 will still provide the upper bound for the information storage capacity per synapse.

Comparison with Poirazi and Mel

In a recent paper, Poirazi and Mel (2001) addressed the memory capacity of neuronal connectivity. For given numbers of different presynaptic inputs and synapses on a postsynaptic neuron, they calculated the number of different ways of distributing those synapses among the inputs. Two distributions of synapses are considered different if they lead to different computations performed by the postsynaptic neuron. Therefore, the number of different distributions depends on the mode of synaptic input integration. In the linear mode, the effect of each input on the postsynaptic neuron depends only on the number of synapses that input makes with the neuron but not on the distribution of synapses among dendritic branches. In the nonlinear mode, where dendritic compartments act as separate thresholding units, the distribution of inputs among dendritic branches matters. Poirazi and Mel (2001) found that a nonlinear neuron can encode a larger amount of information than a linear one because rearrangements of inputs between different dendritic branches lead to different computations performed on the inputs.

In this paper, we make two points related to Poirazi and Mel. First, we calculate the number of potential synapses from measurable anatomical parameters. This result is complementary to Poirazi and Mel because the number of potential synapses can be used as an input to their or other models. Second, we use the number of potential synapses to estimate memory capacity. Our expression for the memory capacity is different from that of Poirazi and Mel because we consider a different parameter regime. In particular, the Poirazi and Mel model assumes that each presynaptic input line can form any number of synapses (provided there is a fixed total number of synapses per branch and branches per neuron) with a given postsynaptic neuron. These changes in connectivity require major remodeling of arbor shapes. Therefore, their model is appropriate for information storage on long time scales. Our model considers modifications on time scales of spine remodeling only. Therefore, the maximum number of synapses that can be formed with a given input line is limited by the number of potential synapses formed by that input. The effect of different modes of integration on the information capacity was discussed in the previous section.

Quantitative Characterization of Memory Mechanisms

Understanding the role of different biological mechanisms in learning and memory requires their characterization by various quantitative parameters. One such parameter is the time scale needed for memory formation. For example, spine formation and elimination is faster than major dendritic or axonal branch remodeling

but slower than synaptic strength change. Another important parameter is the information storage capacity of different mechanisms. In this paper, we estimate an upper bound on the information storage capacity due to one candidate mechanism, i.e., the formation and elimination of spines. This estimate can be used to compare this mechanism to others, once quantitative estimates of their capacity become available. Such comparison will help put different memory mechanisms in perspective adding to the difference in time scales, which made dissecting them meaningful in the first place.

Although we estimate an upper bound on the information storage capacity due to spines, its relationship to the "memory capacity" in the colloquial sense remains open. This can be resolved once a better knowledge of how memories are stored becomes available. Moreover, some aspects of connectivity are genetically predetermined thus reflecting memories stored over evolutionary time scales. Our calculation includes these evolutionary memories in the storage capacity, which may run contrary to the intuitive definition of memory. Alternatively, our estimate can be viewed as the amount of information needed to define spine patterns given major dendritic and axonal arbor architecture.

We find that the filling fraction is different from 1/2, which may seem surprising given that $f = 0.5$ maximizes information storage capacity, Equation 8, for a fixed number of potential synapses. This could be explained by the fact that actual synapses and absence of synapses are not symmetric. For example, an existing synapse takes up volume, which is a valuable resource. This could explain why the filling fraction is less than 1/2, provided the brain's contribution to evolutionary fitness is limited by morphologic constraints on volume as well as on the information storage capacity. Another possible explanation is that pyramidal neurons belong to different classes and only a certain class is eligible to synapse onto a given dendrite.

Role of Dendritic Spines

Ever since the discovery of spines (Ramón y Cajal, 1891), their functional role has been debated. Our results support the view that spines help to increase the choice of potential axons that can form synapses on a given dendrite. This point of view has been expressed by Swindale (1981) who wrote: "…spines can be seen as morphological devices that allow axons and dendrites to pursue economically straight courses through the neuropil, and at the same time permit both a high density and specificity of connections." Indeed, the specificity of connections is the ability of a dendrite (axon) to choose its presynaptic (postsynaptic) targets. This feature is captured by the inverse of the filling fraction f^{-1}, that is, the ratio of potential to actual synapses. According to Equation 2, reducing the length of spines S would lead to the reduction of the number of potential synapses N_P. Hence, in order to maintain the specificity of connections (filling fraction f) or the information capacity per synapse, Equation 9 after spine length reduction, it is necessary to reduce the number of synapses N. Alternatively, if the number of synapses is kept the same, reduction of the average spine length would result

in an increase in f, a decrease in specificity, and a decrease in information storage capacity per synapse (see Figure 6).

A similar view has been expressed by Peters and Kaiserman-Abramof (1970), who proposed that spines are needed for the dendrites to reach out and contact axons. In this manner, the axons would not need to zigzag from one neuron to the other, but rather follow a relatively straight path, which is one of the assumptions used in derivation of Equations 2, 3, and 5.

Although our results support the view that spines serve to enhance plasticity of connectivity between axons and dendrites, they do not rule out other possible spine functions such as biochemical compartmentalization (Denk et al., 1996; Koch and Zador, 1993).

Equipartition of Volume between Axons and Dendrites

The significance of our geometrical analysis goes beyond estimating the number of potential synapses, the filling fraction, and the information storage capacity. Because Equation 2 is a mathematical representation of the reciprocal relationship between axons and dendrites, it places physical constraints on brain design. To illustrate how this constraint can lead to nontrivial results, we use it to explain an interesting anatomical observation of volume equipartition between axons and dendrites.

In the gray matter, axons and dendrites occupy approximately equal fractions of the total volume, about 1/3 each (Braitenberg and Schüz, 1998; Chklovskii et al., 2002; Ikari and Hayashi, 1981). This is unlikely to be just a coincidence because the linear dimensions of axons and dendrites are rather different. In a typical neuron, the total length of axons is ten times greater than the total length of dendrites, while the average axonal diameter is three times smaller than dendritic diameter (Braitenberg and Schüz, 1998). Because the volume is proportional to the length times the diameter squared, both types of processes occupy equal fractions. This leaves us with the question, *why should the volumes of the two types of processes be equal?*

We propose that the equipartition of volume between axons and dendrites could arise as a result of optimally choosing lengths of axonal and dendritic processes in order to maximize information storage capacity of synaptic connectivity patterns. Although we do not know whether this consideration was important in the evolution of the brain architecture, we feel that because of the robustness of the result and the simplicity of the derivation, our observation deserves reader's attention. A similar result for the special case of a two-dimensional topographic projection has been previously derived by minimizing the total wiring volume under the constraint of the total number of synapses (Chklovskii, 2000).

We would like to find axonal and dendritic lengths, which maximize the information storage capacity, without increasing the volume of neuropil. To do this, we vary axonal and dendritic lengths per neuron in the expression for information storage capacity per neuron, I (Equation 9). We fix the rest of the neuropil parameters such as the cross-section areas of axons and dendrites A_a and A_d (here by the cross-section area we mean

the area of a cut segment proportional to the diameter squared), number of synapses per neuron N, etc., as well as the total volume of axonal and dendritic processes per neuron $L_a A_a + L_d A_d$.

The information storage capacity I, Equation 9, is a monotonically decreasing function of filling fraction f (Figure 6), which in turn is inversely proportional to the product of axonal and dendritic lengths per neuron, according to Equation 2. Hence, the information storage capacity I is maximal if the product $L_a L_d$ is maximal. Since cross-section areas A_a and A_d are fixed, this also implies that we need to maximize the product of axonal and dendritic volumes per neuron $(L_a A_a)(L_d A_d)$.

For the fixed total volume of axonal and dendritic processes per neuron $L_a A_a + L_d A_d$, the maximum of the product $(L_a A_a)(L_d A_d)$, and hence of the information storage capacity, is achieved when the two volumes are equal. This happens due to a simple mathematical fact that if the sum of the two variables is fixed, the product is maximal when the two variables are equal. This shows that the maximization of memory capacity stored in synaptic connectivity patterns under the constraint of total volume results in the equipartition of volume between axons and dendrites that has been observed in several areas of the rat and mouse brains (Braitenberg and Schüz, 1998; Chklovskii et al., 2002; Ikari and Hayashi, 1981). It would be interesting to see whether this result holds in other brain regions and species.

Conclusion

We have derived an expression for the synaptic filling fraction, f, in terms of measurable anatomical parameters. By using our measurements and previously published data, we evaluate this expression for several cortical areas and species. The filling fraction characterizes plasticity potential due to formation and elimination of spines. We suggest that measurements of the filling fraction, f, could be used to study effects of genetic or developmental (e.g., sensory deprivation) manipulations, as well as pathological conditions or aging on neuronal circuitry.

Experimental Procedures

Surgical Procedures

Materials for the present study came from five adult male long-tailed macaque monkeys (*Macaca fascicularis*) which were all used in other experiments unrelated to the present project. Details of the surgical procedures have been previously published (Hof et al., 1996). Briefly, two adult male *Macaca fascicularis* were anesthetized, and under aseptic conditions, aqueous solutions of the retrograde tracers Fast Blue (FB, 4%; Sigma, St. Louis, MO) or Diamidino Yellow (DY, 4%; Sigma) were injected in areas V2, V4, TEO, and 46 of the left hemisphere, as described elsewhere (Hof et al., 1996). After a recovery time of three weeks to permit optimal retrograde transport, these animals along with the additional three animals (see below) were then deeply anesthetized and perfused transcardially with cold 1% paraformaldehyde in phosphate-buffered saline (PBS) for 1 min followed by 4% paraformaldehyde in PBS for 14 min. All experimental protocols were conducted within the NIH guidelines for animal research and were approved by the Institutional Animal Care and Use Committee (IACUC) at Mount Sinai School of Medicine.

Tissue Preparation and Staining Procedures

In the three animals that did not receive injections, a full serial collection of coronal sections was obtained from the left hemisphere

for analysis of neuronal densities. Details of these procedures are described in a previous study (Hof and Morrison, 1995). Briefly, the entire left hemispheres were cut into 30 μm frozen sections. A 1:10 section series was collected through the hemisphere and stained with cresyl violet.

In the remaining two animals that received tracer injections, approximately 4 mm thick coronal blocks were dissected out of parietal area 7a, and visual areas V1, V2, and V4. These tissues where cut in 400 μm thick sections and retrogradely labeled neurons were loaded with Lucifer Yellow (Molecular Probes, Eugene, OR; 5%, under a DC of 3–8 nA for 10–15 min) (Nimchinsky et al., 1996). Sections containing filled cells were then coverslipped for further microscopic analysis.

Quantitative Analyses

Based on established cyto- and chemoarchitectonic and connectional criteria (Felleman and Van Essen, 1991; Hof and Morrison, 1995; Lewis and Van Essen, 2000a, 2000b), we defined cortical areas V1, V2, V4, and 7a in the occipital and parietal cortex. We obtained neuronal densities from layer III of each region by analyzing three cresyl violet-stained sections 300 μm apart using a systematic-random design to avoid sampling bias due to preferential sampling of large neurons and to provide an equal probability to explore the entirety of the region of interest (Hof and Morrison, 1995).

Lucifer Yellow-loaded neurons were analyzed in areas V1, V2, V4, and 7a on a confocal laser scanning microscope (Zeiss LSM 410). For visualization of Lucifer Yellow, an ArKr 488/568 laser and a 515-565 bandpass emission filter were used. Neurons were located using a Zeiss NeoFluar 16× objective and observed using a Zeiss Apochromat 100× objective with a numerical aperture of 1.4. In order to resolve spine morphology adequately, a zoom factor of 8 was applied. Three neurons were analyzed from each region and spines were sampled from basal dendrites only. The length of each sampled spine was estimated from the outermost visible point on the spine head to a line parallel to the axis of dendritic shaft at the base of the spine. To obtain the value of s in Table 2, the typical dendrite radius was added to the spine length. Spines that were not entirely visible in the optical plane were not measured, and therefore spines that were located directly above or below the dendrite and that were difficult to visualize with precision were not considered in the analysis. Approximately 77 spines were measured on basal dendrites of each neuron accounting for a total of 919 spines.

Derivation of the Expression for the Number of Potential Synapses

In this subsection, we derive a microscopic equation for the density of potential synapses. This derivation relies on the assumption of uniformity of the gray matter components such as axons and dendrites. To satisfy this assumption, we consider volume V whose linear dimensions are greater than the microscopic dimensions of its contents such as diameters of axons and dendrites, spine lengths, interbouton intervals, i.e., few micrometers, yet smaller than the thickness of the cortical layers or the size of the cortical areas, i.e., a few hundred micrometers.

We approximate all of the axonal and dendritic arbors inside volume V by a collection of straight segments. Then we calculate the probability of two such segments (one axonal, one dendritic) to "intersect," i.e., to come within a spine's length of each other. To get the density of potential synapses, we add the probabilities of "intersects" for all axonal and dendritic segments and divide the result by the volume.

Let us calculate the probability P of intersection of two cylinders of given orientation arbitrarily placed inside a large volume V. We assume that the lengths of these cylinders l_a^i and l_d^j are much larger than their diameters, d_a and d_d. Subscripts a and d denote axon and dendrite, respectively, and d_d is the diameter of the cylinder surrounding the dendritic segment with spines (Figure 2). The probability P is a function of the geometrical sizes of cylindrical segments and the angle θ between them.

Intersection happens every time the beginning of the axonal segment falls inside the box (similar to the box in Figure 3, only with angle θ between the segments) around the dendritic segment. The volume of the box equals $2sl_a^i l_d^j \sin\theta$, where $2s = d_a + d_d$. The axonal

diameter is much smaller than diameter of the dendritic segment with spines (Braitenberg and Schüz, 1998), $d_a \ll d_d$, and is neglected in the main text. The intersection probability for two cylindrical segments with angle θ between their axes is,

$$P_{ij}(\theta) = \frac{2sl_a^i l_d^j \sin\theta}{V} \tag{14}$$

The total number of potential synapses inside volume V, N_p^{tot}, can be calculated by adding the above probabilities for all axonal and dendritic branches,

$$N_p^{tot} = \sum_{ij} P_{ij}(\theta_{ij}) = \sum_{ij} \frac{2sl_a^i l_d^j \sin(\theta_{ij})}{V} \tag{15}$$

To proceed further, we need to use some information about the statistics of neuronal branches. If the distribution of angles θ_{ij} is independent of the distributions of sizes of axonal and dendritic segments l_a^i and l_d^j, then the above equation uncouples,

$$N_p^{tot} = \overline{\sin(\theta_{ij})} \frac{2s}{V} \sum_i l_a^i \sum_j l_d^j = \overline{\sin(\theta_{ij})} \, 2s \frac{L_a^{tot} L_d^{tot}}{V} \tag{16}$$

A bar above the sine function denotes the averaging over the distributions of angles among axonal and dendritic branches, and L_a^{tot} and L_d^{tot} stand for the total axonal and dendritic lengths inside volume V, $L_{a,d}^{tot} = \sum_i l_{a,d}^i$. The density of potential synapses is:

$$n_p = \frac{N_p^{tot}}{V} = \overline{\sin(\theta_{ij})} \, 2s\rho_a\rho_d, \tag{17}$$

where $\rho_{a,d} = L_{a,d}^{tot}/V$ are the axonal and dendritic densities (these are length densities and have the dimensionality of μm^{-2}).

Equation 17 is central to this paper. Below we consider some simplifications and generalizations of this equation for particular brain area geometries.

First, taking into account the geometry of brain area, geometry of dendritic trees, and intrinsic and extrinsic axonal projections, it is possible to calculate

$$\overline{\sin(\theta_{ij})} = \int |\sin(\theta)| P_a(\hat{n}_1) P_d(\hat{n}_2) d\Omega_1 d\Omega_2 \tag{18}$$

In these expressions, θ is the angle between two unit vectors $\hat{n}_1$ and $\hat{n}_2$, $P_{a,d}(\hat{n})$ are the probabilities for axonal and dendritic branches to have direction $\hat{n}$, and Ω is the solid angle,

$$\int P_{a,d}(\hat{n}) d\Omega = 1 \tag{19}$$

It is easy to see that in the case where one of the probabilities P_a or P_d is constant (equal to $1/4\pi$ due to the normalization condition, Equation 19), which means that the axonal or dendritic ramifications are isotropic, the averaging over the solid angles can be performed explicitly,

$$\overline{\sin(\theta_{ij})} = \int |\sin(\theta)| \frac{d\Omega}{4\pi} = \frac{\pi}{4} \tag{20}$$

The maximum value of $\overline{\sin(\theta_{ij})}$ is 1, which is achieved only when axons and dendrites are perpendicular to each other (this is the case, for example, for Purkinje neurons in cerebellum and parallel fiber input).

Second, in some cases, it is possible to express the axonal and dendritic densities $\rho_{a,d}$ in terms of more traditional quantities, like average interbouton interval b, density of neurons n, density of boutons n_b, and dendritic and axonal lengths per neuron $L_{a,d}$. Here we consider only the potential synapses between one type of spiny dendrites and one type of axons. The generalization on the case of many axonal and dendritic types is done below. We consider the following potentially useful cases:

- Dendrites and axons inside volume V belong to local neurons, and the entire arbors are contained inside V (with an exception of a small boundary effects).

  In this case, the axonal and dendritic densities are given by

$$\rho_{a,d} = n_{a,d} L_{a,d}, \tag{21}$$

where $n_{a,d}$ stand for densities of neurons that provide axons and dendrites, respectively. These expressions can be used for calculation of density of potential synapses between intrinsic dendrites and axons of pyramidal neurons (in this case, $n_a = n_d = n$ is the density of pyramidal neurons), intrinsic dendrites of pyramidal neurons, and axons of interneurons, etc.

- Dendrites inside volume V belong to nonlocal neurons, and only a certain known fraction of the tree is contained inside V.

  Here, the dendritic density is given by a similar expression

$$\rho_d = n_d L_d, \tag{22}$$

only L_d, in this case, is the average length of the fraction of dendritic tree contained inside volume V, and n_d is the ratio of number of neurons with dendrites inside the considered volume and V. Equation 22 can be used, for example, to determine the density of potential synapses on pyramidal neurons in one stratum of hippocampus. In this case, L_d is the fraction of dendritic length per pyramidal neuron contained inside the considered stratum, and n_d is the ratio of neurons in the stratum pyramidale to the volume of the considered stratum. A similar example is parallel fiber synapse on Purkinje neuron in the molecular layer of cerebellum.

- Axons inside volume V come from nonlocal neurons (extrinsic axons).

$$\rho_a = b^{ext} n_b^{ext} \tag{23}$$

where b^{ext} is the average interbouton interval for extrinsic axons, and n_b^{ext} is the density of boutons on extrinsic axons in volume V. This expression can be used for calculation of a density of potential synapses formed by extrinsic projections in the neocortex and other brain areas.

Third, Equation 17 can be generalized to the case of several axonal and dendritic types. The density of potential synapses between spiny dendrites of type α and axons of type β is given by

$$n_p^{\alpha,\beta} = \left(\overline{\sin(\theta_{ij})}\right)^{\alpha,\beta} 2s^\alpha \rho_a^\beta \rho_d^\alpha \tag{24}$$

The total density of potential synapses on spiny dendrites of type α can be calculated by summing Equation 24 over all axonal types:

$$n_p^\alpha = 2s^\alpha \rho_d^\alpha \sum_\beta \left(\overline{\sin(\theta_{ij})}\right)^{\alpha,\beta} \rho_a^\beta \tag{25}$$

For example, using Equation 25 one can calculate the density of potential synapses on layer III pyramidal neurons in cortical areas, coming from intrinsic and extrinsic projections. We will assume that axonal arbors are isotropic, and

$$\left(\overline{\sin(\theta_{ij})}\right)^{int,ext} = \frac{\pi}{4} \tag{26}$$

In this case Equation 25 has the form:

$$n_p = \frac{\pi}{2} s \rho_d (\rho_a^{int} + \rho_a^{ext}) \tag{27}$$

The densities of axons and dendrites, are given by:

$$\rho_d = n L_d$$
$$\rho_a^{int} = n L_a = b^{int} n_b^{int}$$
$$\rho_a^{ext} = b^{ext} n_b^{ext} \tag{28}$$

and the total axonal density is

$$\rho_a^{int} + \rho_a^{ext} = b^{int} n_b^{int} + b^{ext} n_b^{ext} = b n_b \tag{29}$$

In Equations 28 and 29, n is the density of layer III pyramidal neurons, L_d is the average dendritic length per layer III pyramidal neuron, b^{int} is the average interbouton interval for intrinsic axons, n_b^{int} is the density of boutons of intrinsic axons, b is the overall average interbouton interval, and n_b is the overall density of boutons. Combining Equations 27 and 29 we get,

$$n_p = \frac{\pi}{2} s n L_d b n_b \tag{30}$$

The number of potential synapses per layer III pyramidal neuron, N_p, is equal to:

$$N_p = \frac{n_p}{n} = \frac{\pi}{2} s L_d b n_b \tag{31}$$

Furthermore, bouton density n_b can be related to synapse density n_s. Taking into account that some fraction κ of all boutons makes multiple synaptic connections with an average number m ($m \approx 2$) of synapses per bouton we have,

$$n_b = \frac{n_s}{1 + \kappa (m - 1)} \tag{32}$$

If the fraction of multiple synaptic boutons κ is small, then $n_b \approx n_s$ (one bouton equals one synapse). Substituting this expression into Equation 31 we arrive at Equation 3 of the main text.

References

Amaral, D.G., Ishizuka, N., and Claiborne, B. (1990). Neurons, numbers and the hippocampal network. Prog. Brain Res. *83*, 1–11.

Amir, Y., Harel, M., and Malach, R. (1993). Cortical hierarchy reflected in the organization of intrinsic connections in macaque monkey visual cortex. J. Comp. Neurol. *334*, 19–46.

Bailey, C.H., and Kandel, E.R. (1993). Structural changes accompanying memory storage. Annu. Rev. Physiol. *55*, 397–426.

Baker, R.E., and Van Pelt, J. (1997). Cocultured, but not isolated, cortical explants display normal dendritic development: a long-term quantitative study. Dev. Brain Res. *98*, 21–29.

Bliss, T.V., and Collingridge, G.L. (1993). A synaptic model of memory: long-term potentiation in the hippocampus. Nature *361*, 31–39.

Boss, B.D., Turlejski, K., Stanfield, B.B., and Cowan, W.M. (1987). On the numbers of neurons in fields CA1 and CA3 of the hippocampus of Sprague-Dawley and Wistar rats. Brain Res. *406*, 280–287.

Braitenberg, V., and Schüz, A. (1998). Cortex: Statistics and Geometry of Neuronal Connectivity, 2nd thoroughly rev. Edition (Berlin: Springer).

Budd, J.M. (1998). Extrastriate feedback to primary visual cortex in primates: a quantitative analysis of connectivity. Proc. R. Soc. Lond. B Biol. Sci. *265*, 1037–1044.

Cash, S., and Yuste, R. (1999). Linear summation of excitatory inputs by CA1 pyramidal neurons. Neuron *22*, 383–394.

Chklovskii, D.B. (2000). Optimal sizes of dendritic and axonal arbors in a topographic projection. J. Neurophysiol. *83*, 2113–2119.

Chklovskii, D.B., Schikorski, T., and Stevens, C.F. (2002). Wiring optimization in cortical circuits. Neuron, in press.

Dailey, M.E., and Smith, S.J. (1996). The dynamics of dendritic structure in developing hippocampal slices. J. Neurosci. *16*, 2983–2994.

Darian-Smith, C., and Gilbert, C.D. (1994). Axonal sprouting accompanies functional reorganization in adult cat striate cortex. Nature *368*, 737–740.

Denk, W., Yuste, R., Svoboda, K., and Tank, D.W. (1996). Imaging calcium dynamics in dendritic spines. Curr. Opin. Neurobiol. *6*, 372–378.

Elston, G.N. (2000). Pyramidal cells of the frontal lobe: all the more spinous to think with. J. Neurosci. *20*, 1–4.

Elston, G.N., and Rosa, M.G. (1997). The occipitoparietal pathway of the macaque monkey: comparison of pyramidal cell morphology in layer III of functionally related cortical visual areas. Cereb. Cortex *7*, 432–452.

Elston, G.N., and Rosa, M.G. (1998). Morphological variation of layer III pyramidal neurones in the occipitotemporal pathway of the macaque monkey visual cortex. Cereb. Cortex *8*, 278–294.

Engert, F., and Bonhoeffer, T. (1999). Dendritic spine changes associated with hippocampal long-term synaptic plasticity. Nature *399*, 66–70.

Feldmeyer, D., Egger, V., Lübke, J., and Sakmann, B. (1999). Reliable synaptic connections between pairs of excitatory layer 4 neurones within a single 'barrel' of developing rat somatosensory cortex. J. Physiol. (Lond.) *521*, 169–190.

Felleman, D.J., and Van Essen, D.C. (1991). Distributed hierarchical processing in the primate cerebral cortex. Cereb. Cortex *1*, 1–47.

Greenough, W.T., and Bailey, C.H. (1988). The anatomy of memory - Convergence of results across a diversity of tests. Trends Neurosci. *11*, 142–147.

Greenough, W.T., Larson, J.R., and Withers, G.S. (1985). Effects of unilateral and bilateral training in a reaching task on dendritic branching of neurons in the rat motor-sensory forelimb cortex. Behav. Neural Biol. *44*, 301–314.

Gustafsson, B., and Wigstrom, H. (1990). Long-term potentiation in the hippocampal CA1 region: its induction and early temporal development. Prog. Brain Res. *83*, 223–232.

Harris, K.M., and Stevens, J.K. (1989). Dendritic spines of CA 1 pyramidal cells in the rat hippocampus: serial electron microscopy with reference to their biophysical characteristics. J. Neurosci. *9*, 2982–2997.

Harris, R.M., and Woolsey, T.A. (1981). Dendritic plasticity in mouse barrel cortex following postnatal vibrissa follicle damage. J. Comp. Neurol. *196*, 357–376.

Hellwig, B., Schüz, A., and Aertsen, A. (1994). Synapses on axon collaterals of pyramidal cells are spaced at random intervals: a Golgi study in the mouse cerebral cortex. Biol. Cybern. *71*, 1–12.

Hof, P.R., and Morrison, J.H. (1995). Neurofilament protein defines regional patterns of cortical organization in the macaque monkey visual system: a quantitative immunohistochemical analysis. J. Comp. Neurol. *352*, 161–186.

Hof, P.R., Ungerleider, L.G., Webster, M.J., Gattass, R., Adams, M.M., Sailstad, C.A., and Morrison, J.H. (1996). Neurofilament protein is differentially distributed in subpopulations of corticocortical projection neurons in the macaque monkey visual pathways. J. Comp. Neurol. *376*, 112–127.

Ikari, K., and Hayashi, M. (1981). Aging in the neuropil of cerebral cortex—a quantitative ultrastructural study. Folia Psychiatr. Neurol. Jpn. *35*, 477–486.

Jones, T.A. (1999). Multiple synapse formation in the motor cortex opposite unilateral sensorimotor cortex lesions in adult rats. J. Comp. Neurol. *414*, 57–66.

Koch, C., and Zador, A. (1993). The function of dendritic spines: devices subserving biochemical rather than electrical compartmentalization. J. Neurosci. *13*, 413–422.

Lendvai, B., Stern, E.A., Chen, B., and Svoboda, K. (2000). Experience-dependent plasticity of dendritic spines in the developing rat barrel cortex in vivo. Nature *404*, 876–881.

Lewis, J.W., and Van Essen, D.C. (2000a). Mapping of architectonic subdivisions in the macaque monkey, with emphasis on parieto-occipital cortex. J. Comp. Neurol. *428*, 79–111.

Lewis, J.W., and Van Essen, D.C. (2000b). Corticocortical connections of visual, sensorimotor, and multimodal processing areas in the parietal lobe of the macaque monkey. J. Comp. Neurol. *428*, 112–137.

Madison, D.V., Malenka, R.C., and Nicoll, R.A. (1991). Mechanisms underlying long-term potentiation of synaptic transmission. Annu. Rev. Neurosci. *14*, 379–397.

Magee, J.C., and Cook, E.P. (2000). Somatic EPSP amplitude is independent of synapse location in hippocampal pyramidal neurons. Nat. Neurosci. *3*, 895–903.

Maletic-Savatic, M., Malinow, R., and Svoboda, K. (1999). Rapid dendritic morphogenesis in CA1 hippocampal dendrites induced by synaptic activity. Science *283*, 1923–1927.

Malinow, R., Mainen, Z.F., and Hayashi, Y. (2000). LTP mechanisms: from silence to four-lane traffic. Curr. Opin. Neurobiol. *10*, 352–357.

Markram, H., Lübke, J., Frotscher, M., Roth, A., and Sakmann, B. (1997). Physiology and anatomy of synaptic connections between thick tufted pyramidal neurones in the developing rat neocortex. J. Physiol. (Lond.) *500*, 409–440.

Nimchinsky, E.A., Hof, P.R., Young, W.G., and Morrison, J.H. (1996). Neurochemical, morphologic, and laminar characterization of cortical projection neurons in the cingulate motor areas of the macaque monkey. J. Comp. Neurol. *374*, 136–160.

O'Rourke, N.A., and Fraser, S.E. (1990). Dynamic changes in optic fiber terminal arbors lead to retinotopic map formation: an in vivo confocal microscopic study. Neuron *5*, 159–171.

Page, T.L., Einstein, M., Duan, H., He, Y., Flores, T., Rolshud, D., Erwin, J.M., Wearne, S.L., Morrison, J.H., and Hof, P.R. (2002). Morphological alterations in neurons forming corticocortical projections in the neocortex of aged patas monkeys. Neurosci. Lett. *317*, 37–41.

Peters, A., and Kaiserman-Abramof, I.R. (1970). The small pyramidal neuron of the rat cerebral cortex. The perikaryon, dendrites and spines. Am. J. Anat. *127*, 321–355.

Petit, T.L., LeBoutillier, J.C., Gregorio, A., and Libstug, H. (1988). The pattern of dendritic development in the cerebral cortex of the rat. Brain Res. *469*, 209–219.

Poirazi, P., and Mel, B.W. (2001). Impact of active dendrites and structural plasticity on the memory capacity of neural tissue. Neuron *29*, 779–796.

Purves, D., and Hadley, R.D. (1985). Changes in the dendritic branching of adult mammalian neurones revealed by repeated imaging in situ. Nature *315*, 404–406.

Purves, D., Hadley, R.D., and Voyvodic, J.T. (1986). Dynamic changes in the dendritic geometry of individual neurons visualized over periods of up to three months in the superior cervical ganglion of living mice. J. Neurosci. *6*, 1051–1060.

Rajan, I., and Cline, H.T. (1998). Glutamate receptor activity is required for normal development of tectal cell dendrites in vivo. J. Neurosci. *18*, 7836–7846.

Rajan, I., Witte, S., and Cline, H.T. (1999). NMDA receptor activity stabilizes presynaptic retinotectal axons and postsynaptic optic tectal cell dendrites in vivo. J. Neurobiol. *38*, 357–368.

Ramón y Cajal, S. (1891). Sur la structure de l'écorce cérébrale de quelques mammifères. La Cellule *7*, 125–176.

Ramón y Cajal, S. (1893). Neue Darstellung vom histologischen Bau des Centralnervensystems. Arch. Anat. Physiol. Anat. Abt. Suppl., 319–428.

Rieke, F., Warland, D., de Ruyter van Stevenink, R., and Bialek, W. (1997). Spikes: Exploring the Neural Code (Cambridge, MA: MIT Press).

Schüz, A., and Palm, G. (1989). Density of neurons and synapses in the cerebral cortex of the mouse. J. Comp. Neurol. *286*, 442–455.

Shannon, C.E., and Weaver, W. (1949). The mathematical theory of communication (Urbana, IL: University of Illinois Press).

Shepherd, G.M., and Harris, K.M. (1998). Three-dimensional structure and composition of CA3→CA1 axons in rat hippocampal slices: implications for presynaptic connectivity and compartmentalization. J. Neurosci. *18*, 8300–8310.

Shepherd, G.M.G., Raastad, M., and Andersen, P. (2002). General and variable features of varicosity spacing along unmyelinated axons in the hippocampus and cerebellum. Proc. Natl. Acad. Sci. USA, in press.

Sorra, K.E., and Harris, K.M. (1993). Occurrence and three-dimensional structure of multiple synapses between individual radiatum axons and their target pyramidal cells in hippocampal area CA1. J. Neurosci. *13*, 3736–3748.

Spacek, J., and Hartmann, M. (1983). Three-dimensional analysis of dendritic spines. I. Quantitative observations related to dendritic spine and synaptic morphology in cerebral and cerebellar cortices. Anat. Embryol. *167*, 289–310.

Stern, J.E., and Armstrong, W.E. (1998). Reorganization of the dendritic trees of oxytocin and vasopressin neurons of the rat supraoptic nucleus during lactation. J. Neurosci. *18*, 841–853.

Swindale, N.V. (1981). Dendritic spines only connect. Trends Neurosci. *4*, 240–241.

Tanzi, E. (1893). I fatti i le induzione nell'odierna istologia del sistema nervoso. Riv. Sper. Freniatr. *19*, 419–472.

Toni, N., Buchs, P.A., Nikonenko, I., Bron, C.R., and Muller, D. (1999). LTP promotes formation of multiple spine synapses between a single axon terminal and a dendrite. Nature *402*, 421–425.

Trommald, M., Jensen, V., and Andersen, P. (1995). Analysis of dendritic spines in rat CA1 pyramidal cells intracellularly filled with a fluorescent dye. J. Comp. Neurol. *353*, 260–274.

Valverde, F. (1978). The organization of area 18 in the monkey. A Golgi study. Anat. Embryol. (Berl.) *154*, 305–334.

West, M.J., Danscher, G., and Gydesen, H. (1978). A determination of the volumes of the layers of the rat hippocampal region. Cell Tissue Res. *188*, 345–359.

Witte, S., Stier, H., and Cline, H.T. (1996). In vivo observations of timecourse and distribution of morphological dynamics in Xenopus retinotectal axon arbors. J. Neurobiol. *31*, 219–234.

Wong, W.T., Faulkner-Jones, B.E., Sanes, J.R., and Wong, R.O. (2000). Rapid dendritic remodeling in the developing retina: dependence on neurotransmission and reciprocal regulation by Rac and Rho. J. Neurosci. *20*, 5024–5036.

Woolley, C.S. (1999). Structural plasticity of dendrites. In Dendrites, G. Stuart, N. Spruston, and M. Häusser, eds. (Oxford: Oxford University Press), pp. 339–364.

Yankova, M., Hart, S.A., and Woolley, C.S. (2001). Estrogen increases synaptic connectivity between single presynaptic inputs and multiple postsynaptic CA1 pyramidal cells: A serial electron-microscopic study. Proc. Natl. Acad. Sci. USA *98*, 3525–3530.